Earth and Planetary Science Letters 307 (2011) 103–112

Contents lists available at ScienceDirect

Earth and Planetary Science Letters

journal homepage: www.elsevier.com/locate/epsl

Model, proxy and isotopic perspectives on the East African Humid Period

Jessica E. Tierney [a,*], Sophie C. Lewis [b], Benjamin I. Cook [a,c], Allegra N. LeGrande [c], Gavin A. Schmidt [c]

[a] Lamont-Doherty Earth Observatory of Columbia University, Palisades, NY 10964, USA
[b] Research School of Earth Sciences, The Australian National University, ACT 0200, Australia
[c] NASA Goddard Institute for Space Studies and Center for Climate Systems Research, Columbia University, 2880 Broadway, New York, NY 10025, USA

ARTICLE INFO

Article history:
Received 11 January 2011
Received in revised form 11 April 2011
Accepted 26 April 2011
Available online 23 May 2011

Editor: G. Henderson

Keywords:
East Africa
African Humid Period
hydrogen isotopes
Holocene climate
African climate
isotope-enabled climate model

ABSTRACT

Both North and East Africa experienced more humid conditions during the early and mid-Holocene epoch (11,000–5000 yr BP; 11–5 ka) relative to today. The North African Humid Period has been a major focus of paleoclimatic study, and represents a response of the hydrological cycle to the increase in boreal summer insolation and associated ocean, atmosphere and land surface feedbacks. Meanwhile, the mechanisms that caused the coeval East African Humid Period are poorly understood. Here, we use results from isotope-enabled coupled climate modeling experiments to investigate the cause of the East African Humid Period. The modeling results are interpreted alongside proxy records of both water balance and the isotopic composition of rainfall. Our simulations show that the orbitally-induced increase in dry season precipitation and the subsequent reduction in precipitation seasonality can explain the East African Humid Period, and this scenario agrees well with regional lake level and pollen paleoclimate data. Changes in zonal moisture flux from both the Atlantic and Indian Ocean account for the simulated increase in precipitation from June through November. Isotopic paleoclimate data and simulated changes in moisture source demonstrate that the western East African Rift Valley in particular experienced more humid conditions due to the influx of Atlantic moisture and enhanced convergence along the Congo Air Boundary. Our study demonstrates that zonal changes in moisture advection are an important determinant of climate variability in the East African region.
© 2011 Elsevier B.V. All rights reserved.

1. Introduction

During the early and mid-Holocene epoch (11–5 ka), paleohydrological data suggest that both North and East Africa experienced more pluvial conditions relative to the present day (Gasse, 2000; Peyron et al., 2000; Street and Grove, 1979). In North Africa, this Holocene pluvial period is often referred to as the "African Humid Period" (AHP, deMenocal et al., 2000), and the hydrological changes were extreme; pollen evidence indicates that the Saharan desert was transformed into an open grass savannah, dotted with shrub and tree species that today grow hundreds of kilometers to the South (Jolly et al., 1998; Kröpelin et al., 2008; Ritchie et al., 1985). Though the abruptness with which the AHP ended near 5 ka is still a matter of debate (Adkins et al., 2006; deMenocal et al., 2000; Kröpelin et al., 2008; Liu et al., 2007; Renssen et al., 2006), the cause of the AHP is fairly well understood: increased solar insolation in the North African subtropics during the boreal summer season resulted in enhanced transport of water vapor from the Atlantic ocean onto land (Kutzbach and Otto-Bliesner, 1982), and changes in the meridional sea-surface temperature gradient in the North Atlantic accompanied by wind-evaporation feedbacks augmented this response (Kutzbach and Liu, 1997; Liu et al., 2004; Zhao et al., 2007). Vegetation feedbacks may have further fomented humid conditions (Peyron et al., 2006).

The extension of the AHP along the East African Rift – as far south as 9°S – is not as well understood. In modeling simulations, the reduction in early to mid-Holocene insolation during the southern hemisphere rainy season (November–March) weakens the southern tropical monsoons and promotes drier conditions (Liu et al., 2004). However, lakes situated far south of the equator, such as Lake Rukwa (8°S, Vincens et al., 2005) and Lake Cheshi (9°S, Stager, 1988) experienced higher lake levels in the early and mid-Holocene than at present. Isotopic proxy reconstructions from the Congo Basin (Schefuß et al., 2005) and Lake Tanganyika (Tierney et al., 2008) also point towards more pluvial conditions in the southern African tropics, and do not suggest that hydroclimate responded to the meridional migration in the Intertropical Convergence Zone (ITCZ), unlike other areas of the tropics (e.g. Haug et al., 2001).

Here, we adopt a combined model and proxy approach in order to understand the cause of the enigmatic "East African Humid Period." We review the patterns of hydrological balance and reconstructed changes in the isotopes of precipitation provided by the proxy data, and then explore mechanisms behind the observed changes using simulations conducted with the fully coupled, isotope-enabled NASA Goddard Institute for Space Studies (GISS) ModelE-R. The stable isotopes of water (HHO, HDO, and $HH^{18}O$; expressed in per mil notation as δD and $\delta^{18}O$) serve as tracers of the hydrological cycle, as

* Corresponding author.
E-mail address: tierney@ldeo.columbia.edu (J.E. Tierney).

0012-821X/$ – see front matter © 2011 Elsevier B.V. All rights reserved.
doi:10.1016/j.epsl.2011.04.038

they preserve an integrated history of water and water vapor. The model and proxy inferences of isotopic changes across the Holocene complement the hydrological information provided by the lake level proxies and simulated water balance, as they offer large-scale and physically consistent insight into atmospheric processes such as the transport of water vapor from ocean to land (LeGrande and Schmidt, 2009) and shifts in the source of precipitation (Lewis et al., 2010).

2. Overview of East African climatology

Two major convergence zones define precipitation climatology in tropical and East Africa: the east–west-oriented ITCZ, and the northeast–southwest-oriented Congo Air Boundary (CAB; Fig. 1). The CAB marks the confluence of Atlantic Ocean-derived moisture with Indian Ocean-derived moisture and its location is determined partly by orographical constraints including the Ethiopian and Kenyan Highlands. Convergent, unstable air within the CAB serves as an important source of seasonal rainfall to Ethiopia (Levin et al., 2009) as well as the western branch of the East African Rift Valley and most of western Tanzania (Mapande and Reason, 2005). The Horn of Africa and coastal East Africa are isolated orographically from convergence along the CAB, and consequently these regions are more arid. The aridity of easternmost Africa also reflects micro-orographical effects such as leeward rain shadows east of Mt. Kenya and Mt. Kilimanjaro, and the influence of divergent, dry lower-level winds that move parallel to the East African shore from June–September and December–February (Nicholson, 1996).

The migration of the ITCZ and CAB through the annual cycle skews the seasonal distribution of precipitation in East Africa towards October–May (Fig. 1). The majority of the region experiences a well-pronounced dry season from June–August, followed by either two rainy seasons for areas north of and close to the equator (with peak rains in November and April) or an extended rainy season from October–May for areas farther south of the equator. On interannual timescales, East African precipitation variability is sensitive to both Atlantic Ocean and Indian Ocean climate dynamics. For areas receiving precipitation from the CAB, interannual changes in Atlantic Ocean sea surface temperatures (SSTs) and SST gradients can modulate the strength of the trade winds and the advection of moisture into equatorial Africa; a flattening of the meridional gradient in Atlantic SSTs (e.g. warmer South Atlantic SSTs) typically results in anomalously high precipitation rates (Camberlin et al., 2001). In easternmost tropical Africa, shifts in Walker circulation over the Indian Ocean basin – particularly during the boreal fall after the cessation of the summer Indian monsoon – cause large interannual fluctuations in precipitation. A flattening of the zonal SST gradient in the Indian Ocean and subsequent reversal of Walker circulation typically causes anomalous convergence and rainfall in the western Indian Ocean extending into easternmost Africa. Such shifts in zonal circulation can be caused by anomalously warm SSTs in the western Indian Ocean (Goddard and Graham, 1999; Ummenhofer et al., 2009), positive Indian Ocean Dipole events (Saji et al., 1999), and the El Niño-Southern Oscillation (Camberlin et al., 2001; Nicholson and Kim, 1997).

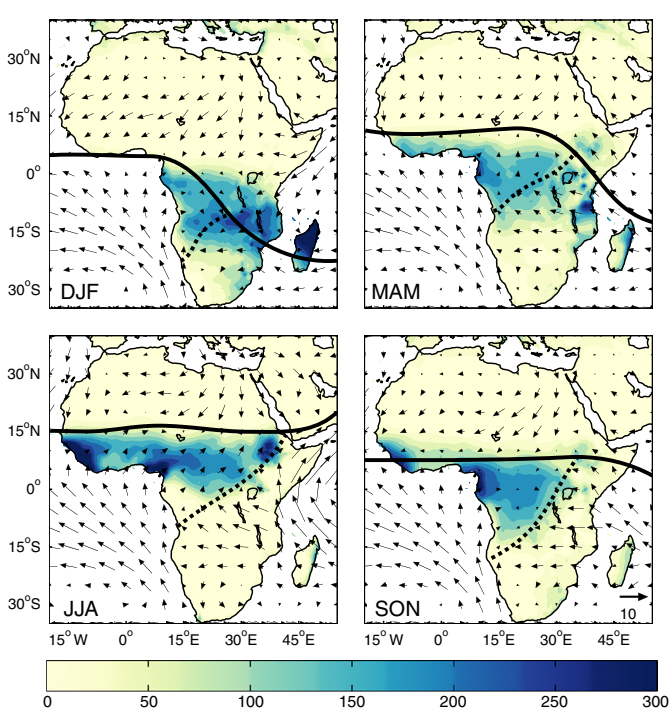

Fig. 1. Seasonal precipitation and wind climatology for tropical Africa, including precipitation rates (mm/month, in color; UEA CRU TS 2.1, Mitchell and Jones, 2005), surface winds (Kalnay et al., 1996), and the approximate locations of the Intertropical Convergence Zone (ITCZ, solid line) and Congo Air Boundary (CAB; dotted line).

3. Methods

3.1. Modeling approach

Simulations were conducted with the M20 version of the coupled ocean–atmosphere NASA GISS ModelE-R, which has a horizontal resolution of $4° \times 5°$, 20 vertical levels up to 0.1 hPa in the atmosphere (Schmidt et al., 2006) and a 13-layer Russell ocean model (Hansen et al., 2007). Atmospheric advection uses the quadratic upstream scheme, with 9 moments advected in addition to mean quantities. The ocean component is non-Boussinesq, mass conserving and uses natural boundary conditions at the free surface. Water isotope tracers ($H_2^{16}O$, $HD^{16}O$, and $H_2^{18}O$, expressed in per mil (‰) notation as δD and $\delta^{18}O$) are incorporated into the atmosphere, ocean, land surface and sea ice and are tracked through all phases of the hydrological cycle, with an appropriate fractionation applied at each phase change (Schmidt et al., 2005, 2007).

We compare the pre-industrial control (0K) simulation with the 6000 yr BP (6K) simulation that was conducted as part of previously-published Holocene "timeslice" experiments (LeGrande and Schmidt, 2009). For the 6K experiment, seasonal insolation was determined according to orbital parameters (Berger and Loutre, 1991) and greenhouse gas concentrations were prescribed based on ice core reconstructions (Brook et al., 2000; Indermühle et al., 1999; Sowers et al., 2003). The experiment was run for 500 years, and we use the average of the last 100 years of data as the basis of our results and interpretations. 6K–0K differences were tested for significance using a student's *t* test.

This version of ModelE contains a simple variable lakes scheme, which we use to calculate 6K–0K lake mass anomalies. Lakes contain two layers; the first layer has a minimum depth of 1 m, and the second, deeper layer is unlimited. Lakes are given pre-defined sill depths based on topography. The mass of the lakes depends on precipitation, evaporation, lake ice melt and freeze, river inflow from upstream boxes and river outflow to downstream boxes. There is heat diffusion at the interface of the two lake layers, and convective overturning will occur if the temperature stratification is unstable. The model can also "grow" new lakes in grid boxes that receive river inflow from upstream boxes and have no outlet, or have a pre-defined sill depth that is not exceeded.

To diagnose shifts in moisture sources to tropical Africa, we utilized vapor source distribution (VSD) tracers (Lewis et al., 2010), which are analogous to non-fractionating water isotope tracers and are a generalization of the "painted water" approach (Koster et al.,

1986). The precipitation source distribution (PSD) used in this study is a subset of the VSD and is defined by where water vapor condenses into liquid, thus specifically traces the origin of vapor that becomes precipitation. Spherical harmonics are used as the VSD basis functions, which are not anchored to geographical boundaries and require no prior definition of regions. The 144 VSD tracers are resolved at T11 resolution, with an effective horizontal resolution of ca. 8°×10°. These tracers are computationally expensive and slow the model by a factor of 10, so we conducted the VSD experiments with atmosphere-only simulations at 0K and 6K using prescribed SST and sea ice conditions from the parallel coupled simulation. A 0K coupled simulation with the VSDs enabled was conducted to test the validity of the atmosphere-only simulations, and only small differences in precipitation source distributions were observed (Lewis et al., 2010).

3.2. Proxy reconstructions

For continent-wide estimates of water balance, we refer to the Oxford Lake-Level Database (OLLD; Street-Perrott et al., 1989). The OLLD classifies relative lake levels into three categories: "low" = lake is dry and/or at its most saline, and/or within 0–15% of its total altitudinal range of fluctuation, "intermediate" = lake is within 15–70% of its altitudinal range and/or ambiguously rising or falling, and "high" = lake is within 70–100% of its altitudinal range and/or overflowing, and/or at its deepest/freshest state. So as to include more recently-published lake level or lake salinity reconstructions, we added data from Lake Bosumtwi (6°30′N, 1°25′W, Shanahan et al., 2006), Lake Edward (0°, 29°30′E, Russell et al., 2003), Lake Malawi (9–14°S, 34–35°E Finney and Johnson, 1991), Lake Victoria (1°S, 33°E Stager et al., 2003; Talbot and Laerdal, 2000), and Lake Challa (3°19′S, 37°42′E, Verschuren et al., 2009) using the same classification scheme (Fig. 2).

For past estimates of the isotopes of precipitation, we utilized three continental sedimentary records of the deuterium/hydrogen composition of leaf waxes (δD_{wax}) from the southern African tropics. The first leaf wax record is from a marine sediment core near the Congo River Delta (5°35.3′S, 11°13.30′E), which integrates plant waxes from throughout the Congo basin (Schefuß et al., 2005). The second and third records are from lake sediment cores from Lake Tanganyika (6°42′S, 29°50′E, Tierney et al., 2008) and Lake Challa (3°19′S, 37°42′E, Tierney et al., 2011, Fig. 2). Sedimentary transect

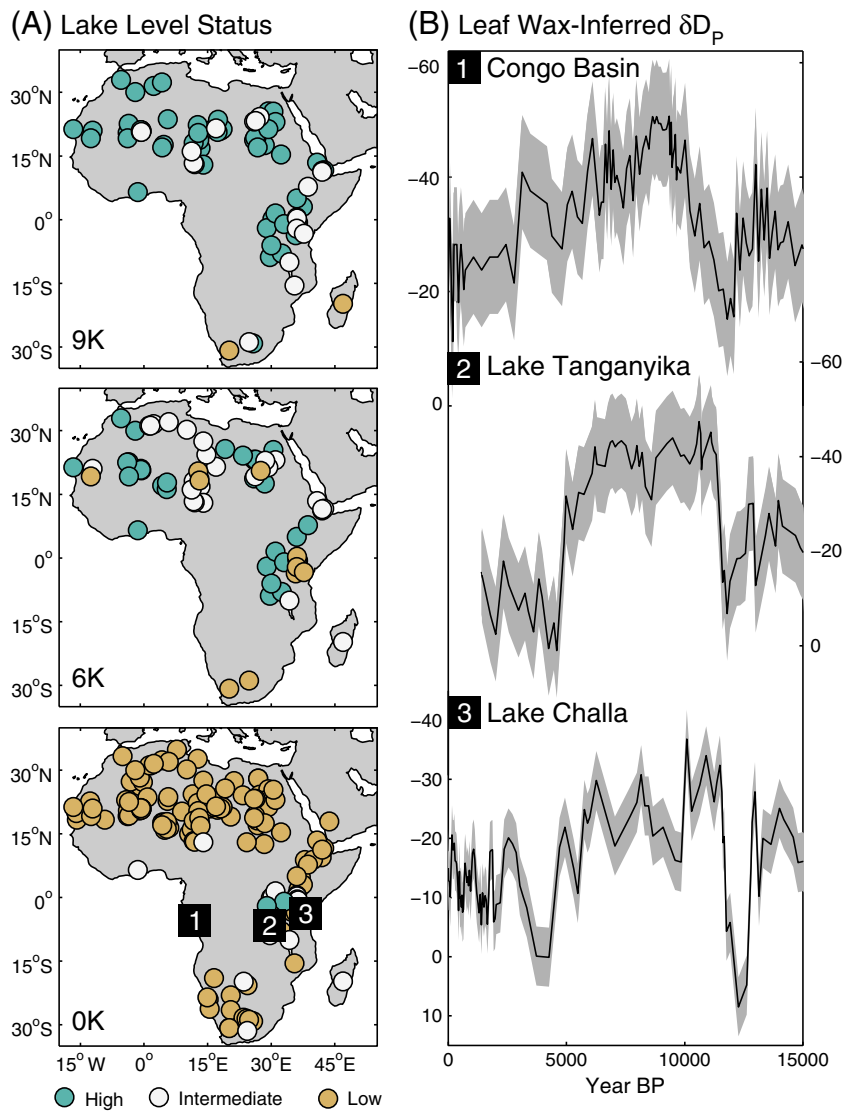

Fig. 2. (A) Proxy lake level reconstructions from the Oxford Lake-Level Database (Street-Perrott et al., 1989), updated with more recent lake level reconstructions as mentioned in the main text, serve as a reference point for Holocene changes in water balance. (B) Leaf wax isotopic proxy data reflect past changes in δD_P at three locations across the African tropics: 1 = Schefuß et al. (2005), 2 = Tierney et al. (2008), 3 = Tierney et al. (2011). Data shown here are converted from raw leaf wax δD values to estimates of δD_P as described in the main text; error bars represent the 1σ uncertainty associated with the δD_P estimation. 'Year BP' indicates calendar years before AD 1950.

studies show that δD_{wax} linearly tracks the hydrogen isotopic composition of precipitation (δD_P) with a relatively consistent offset – i.e. 'apparent fractionation (ε)' – in most climates and biomes (Hou et al., 2008; Polissar and Freeman, 2010; Sachse et al., 2004), and thus acts as a proxy for δD_P. Changes in vegetation type (i.e., the mean source vegetation for the leaf waxes) as well as relative humidity have potential to exert second-order effects of the δD_P-δD_{wax} relationship (Hou et al., 2008; Smith and Freeman, 2006). However, the empirical sensitivity of apparent ε to relative humidity is low; compiled transect data suggest that a ca. 20% change in relative humidity causes a ca. 10‰ change in ε (Hou et al., 2008; Tierney et al., 2010), and within some biomes there is no apparent sensitivity of ε to relative humidity (Feakins and Sessions, 2010). The relatively small impact of relative humidity on ε may indicate that plants use hydrogen from stem water or another stored source rather than exclusively leaf water in synthesizing leaf waxes (McInerney et al., 2011).

Vegetation changes also need to be large to impart bias in the δD_{wax} proxy, and this is likely not an issue at the Congo or Challa sites, as carbon isotope data suggest that these areas have largely remained stable ecosystems of rainforest and open grassland savanna, respectively, over the past 10,000 years (Schefuß et al., 2005; Sinninghe Damsté et al., 2011). Pollen and carbon isotope data from Lake Tanganyika do suggest a shift in biome between the Early and Late Holocene, most likely from a relatively closed miombo woodland forest to a more open grass savanna (Tierney et al., 2010; Vincens et al., 1993a,b). Previous comparison of paired carbon and hydrogen isotope data at Lake Tanganyika concluded that vegetation change likely did not produce a direct effect on δD_{wax}, as the mean apparent ε for the dominant vegetation types near the lake (C_3 trees and shrubs vs. C_4 grasses) is thought to be relatively similar (Tierney et al., 2010). A change in the "openness" of the landscape as a consequence of the biome shift may have amplified the early to mid-Holocene δD_{wax} signal at Tanganyika by decreasing the amount of soil or leaf water evaporation — i.e. via the "relative humidity effect" discussed above. Based on empirical transect data (Hou et al., 2008), this effect could account for approximately a third of the observed depletion in δD_{wax} if we assume a somewhat improbably large change in relative humidity (e.g. a 15–20% increase). Thus while secondary amplification of the δD_{wax} signal at Tanganyika cannot be discounted, the majority of the variance in δD_{wax} at this site is likely due to large changes in δD_P.

In some tropical plant species, wax production occurs only during periods of leaf expansion (Neinhuis and Barthlott, 1997), which would cause the δD_{wax} proxy to preferentially represent δD_P whenever plant growth begins. Indeed, in a study of European barley leaves Sachse et al. (2010) determined that the leaf wax δD signal is "locked in" early during leaf development and thus can capture seasonal variation in δD_P. Since precipitation climatology in East Africa is highly seasonal, we speculate that the δD_{wax} proxy will be biased towards the onset of the rainy season in October–November, when many plant species begin or resume growing after limited or no growth during the dry season.

To facilitate comparison with model output as well comparison between the proxy records, we converted the δD_{wax} data to estimates of paleo-δD_P by fitting the mean δD_{wax} of the last 3500 years to the modern instrumental value of δD_P. For the Congo Basin record, we used weighted mean δD_P from the IAEA monitoring station in Kinshasa (4.37°S, 15.25°E), which is -25.2 ± 8‰. Given a mean Late Holocene δD_{wax} of -141 ± 4‰ this corresponds to an apparent ε of -119 ± 9‰, which was then applied to the time series to convert from δD_{wax} to δD_P. In the case of Lake Tanganyika, no direct measurements of δD_P are available so we used the reported average δD of Tanganyika tributaries, which is -10 ± 8‰ (Craig et al., 1974). Given the Late Holocene δD_{wax} mean of -101 ± 5‰ this yields an apparent ε of -91 ± 9‰. For the Lake Challa record, we used the average δD of river, stream and tap water samples between 2 and 4°S, 37–39°E, 300–1000 m elevation ($n = 9$) that were collected as part of a comprehensive study of the isotopic composition of East African waters (Levin et al., 2009). This resulted in a mean δD_P of -13 ± 3‰. With a Late Holocene mean of -104 ± 4‰, apparent ε is -92 ± 5‰.

The Congo Basin estimate of apparent ε is much lower than the estimates for Lake Tanganyika and Lake Challa, but this is primarily a reflection of the specific leaf wax compound that was analyzed. The Congo Basin study analyzed δD_{wax} on the C_{29} *n*-alkane, whereas the Tanganyika and Challa studies analyzed the C_{28} *n*-acid. Higher plant *n*-alkanes and *n*-alkanoic acids are synthesized from the same molecular precursor in plants and are both components of epicuticular leaf wax, but the decarboxylation step involved in synthesizing the *n*-alkane compounds appears to impart a systematically lower δD value as compared to its equivalent *n*-alkyl fatty acid, with $\varepsilon_{alkane-acid} = 25$‰ (Chikaraishi and Naraoka, 2007). In *n*-acid space, the apparent ε for the Congo would be -97‰; close to the estimates for Tanganyika and Challa.

The 1σ uncertainty plotted with our inferred paleo-δD_P estimates (Fig. 2) includes the compounded 1σ analytical error (2‰) and the 1σ error of the apparent ε estimations (which in turn includes the standard deviation of the Late Holocene means and the 1σ errors in the δD_P estimates) and is 10‰, 10‰, and 5‰ for the Congo Basin, Lake Tanganyika, and Lake Challa respectively.

4. Results and discussion

4.1. GISS ModelE-R performance in Africa

Prior to interpreting the simulated 6K–0K anomalies, we first compare the mean of the last 100 years of the control simulation with modern precipitation and isotope climatology for tropical Africa as an assessment of GISS ModelE-R's ability to simulate African hydrology (Fig. 3). In spite of its coarse resolution, the M20 version of GISS ModelE-R generally simulates mean annual precipitation in tropical Africa well. ModelE-R does overestimate precipitation rates in easternmost Africa;

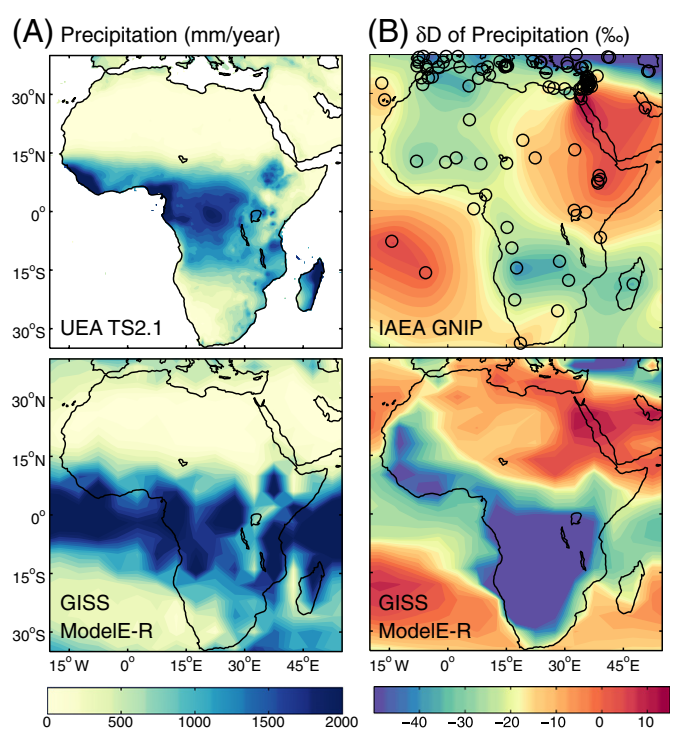

Fig. 3. (A) A comparison between instrumental (UEA CRU TS2.1 gridded precipitation; Mitchell and Jones, 2005) and simulated annual precipitation rates in GISS ModelE-R in the control (0K) run. (B) A comparison between instrumental estimates of the weighted mean annual hydrogen isotopic composition of precipitation (δD_P; interpolated between the IAEA monitoring stations (IAEA/WMO, 2006) marked as circles) and 0K δD_P simulated by GISS ModelE-R.

this most likely reflects the inability of a 4° by 5° model to capture the small orographical features contributing to aridity in this region (see Section 2). GISS ModelE-R also underestimates the asymmetry between the "short rains" season (October–December) and the "long rains" season (March–May) in East Africa, but simulates the timing of seasonal changes in precipitation correctly. Since these biases in East African precipitation are largely related to the resolution of the model, they affect the 6K and 0K simulations similarly, and so we consider the precipitation anomaly patterns robust.

The simulated weighted mean annual isotopes of precipitation in GISS ModelE-R capture the large-scale structures evident in the instrumental data (weighted mean annual IAEA station data, IAEA/WMO, 2006) – including the enriched δD_P over the Red Sea and Saudi Arabia – but clearly overestimate the amount of depletion in δD_P in the Congo Basin and South Africa (Fig. 3). The subdued inland gradient evident in the instrumental IAEA data suggests that transpiration of water by the Congo rainforest – which proceeds with little effective isotopic discrimination – limits the expression of the "continentality effect" (e.g., the progressive rainout of heavy isotopes as a parcel of water vapor travels farther into the interior of a continent) in tropical Africa (Rozanski et al., 1993). The model does not capture this trend, perhaps due to a limitation of the land-surface component of the model, such as the parameterization of canopy interception of falling rain vis-a-vis transpiration. As GISS ModelE-R does not include a dynamic vegetation model, the excessive depletion of δD_P affects both the 6K and 0K simulations similarly and we assume that anomalies in δD_P between the 6K and 0K simulations are meaningful; nonetheless, this inaccuracy suggests that tropical African δD_P within GISS ModelE-R should be interpreted with care.

4.2. On the cause of the East African Humid Period

At 6K, GISS ModelE-R simulates a coherent pattern of hydroclimatic change across most of Africa relative to the 0K control simulation, indicating an increase in Precipitation–Evaporation (P–E) during June–July–August (JJA) and September–October–November (SON), and a decrease in P–E during December–January–February (DJF) and March–April–May (MAM; Fig. 4). These results are consistent with the expectation that changes in insolation in the mid-Holocene – a ca. 5% increase in JJA and ca. 5% decrease in DJF – enhance the Northern Hemisphere summer monsoons (i.e., JJA precipitation) but weaken the southern hemisphere summer monsoons (i.e. DJF precipitation) due to continental cooling and enhanced land–sea contrast (Liu et al., 2004). Given that the rainy season in East Africa spans October–May, the 6K–0K anomalies indicate that precipitation seasonality in East Africa was reduced in the mid-Holocene: there was a wetter dry/transitional season (June–November) and a drier wet season (December–May).

The simulated changes in δD_P in East Africa at 6K follow the changes in P–E, with more depleted rainfall occurring in JJA and SON and more enriched rainfall in DJF and MAM (Fig. 4B). The straightforward relationship between P–E and δD_P suggests an amount effect control on the isotopes of precipitation in East Africa, and the seasonal changes in δD_P scale linearly to changes in precipitation rate in this region. However, the large isotopic depletion

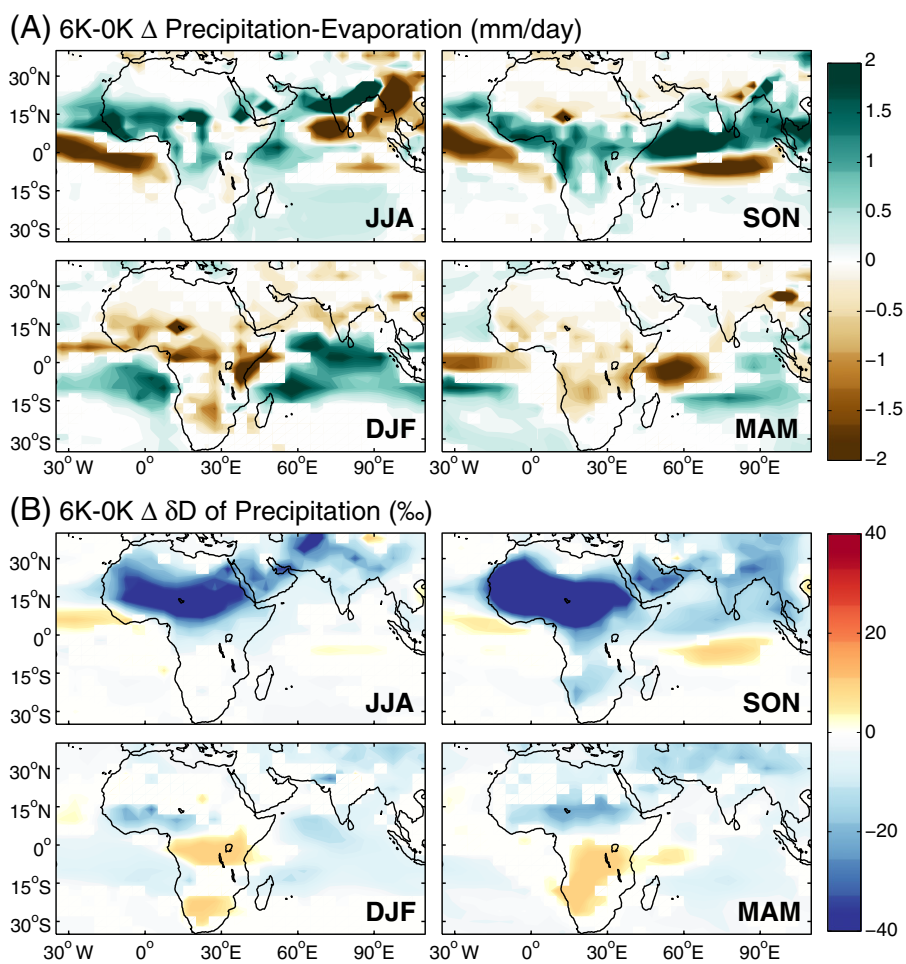

Fig. 4. (A) Simulated seasonal 6K–0K change in Precipitation–Evaporation in Africa and (B) Simulated seasonal 6K–0K change in δD_P in Africa. Only differences significant at the 95% confidence level are shown.

simulated for North Africa at 6K does not scale to the changes in precipitation in that region, and this anomaly – which extends to the equator – may additionally influence the isotopic composition of rain in the northernmost areas of East Africa. Notably, the proxy-inferred changes in mean δD_P in the Congo Basin (−14‰) and at Lake Challa (−8‰) are in better agreement with the simulated changes in δD_P from June–November for the Congo Basin region (8°N–12°S, 10–30°E; −16‰) and East Africa (8°N–12°S, 30°E–45°E; −7‰) rather than the simulated mean annual changes in δD_P (−8‰ for the Congo Basin and −1‰ for East Africa). This may indicate that the δD_{wax} proxy has a seasonal bias, as we assume (see Section 3.2). However, given the limitations of GISS ModelE-R in simulating the isotopes of precipitation over tropical Africa, it is also possible that the depletion at 6K inferred from δD_{wax} reflects a process beyond amount effect that is not well-simulated by the model.

On a mean annual basis, there is a net increase in P–E near the Congo Air Boundary, but for the majority of East Africa increased P–E from June–November is offset by reduced P–E from December–May and the annual P–E anomaly is near-zero or even negative (Fig. 5A). Similarly, mean annual changes in δD_P are close to zero for the East African region (not shown). However, GISS ModelE-R simulates positive mean annual lake mass anomalies in North Africa as well as throughout the East African Rift (Fig. 5C), in general agreement with proxy lake level reconstructions (Fig. 5D). Although precipitation changes are minimal on the mean annual basis, and lake evaporation actually increases as lake areas expands, increased ground runoff (above ground and underground) drives the increase in lake mass in the 6K simulation. Ground runoff, especially underground flow, slowly responds to precipitation changes, and monthly or seasonal anomalies persist in the following months and greatly impact the annual mean. Thus, the simulated rise in lake levels at 6K indicates that the large relative increase in P–E during the dry season has a major and lasting impact on cumulative annual water balance via runoff, whereas the decrease in P–E during the wet season (which is smaller on a relative basis) has less of an impact. This leads to the establishment of higher lake levels in spite of little change in mean annual P–E. Simulated soil moisture, which like lake levels is an integrative measure of hydrological change, also increases at 6K relative to present throughout the Rift Valley with particularly strong anomalies in the Great Lakes region (Fig. 5B). We expect that this increase in perennial soil moisture would have driven shifts in the dominant vegetation in East Africa, and pollen data indicate that this was indeed the case. Early and mid-Holocene pollen data from equatorial East Africa show a dominance of humid semi-deciduous taxa (Beuning and Russell, 2004; Jolly et al., 1997; Kendall, 1969) and farther south, pollen data from Lake Tanganyika and Lake Rukwa show an expansion of miombo woodland species (e.g. *Celtis*, *Uapaca* and *Brachystegia*) at 6K in areas that today are dominated by grass savanna (Vincens et al., 1993b, 2005). These ecosystem shifts require greater water availability, but not necessarily an increase in mean annual P–E. A recent modeling study using the biosphere model BIOME 3.5 demonstrates that by reducing the seasonality of precipitation – and thus reducing the number of consecutive dry days – one can promote an ecosystem shift from grass savanna to woodland miombo and onto humid semi-deciduous taxa in tropical East Africa (Gritti et al., 2010). Our simulations, which suggest an increase in dry season precipitation at 6K but little change in mean annual P–E, are thus fully compatible with the pollen data from East Africa. The overall agreement between the simulated changes in lake mass and soil moisture and the available paleoclimate data suggests that a reduction in precipitation seasonality – in other words, a wetter dry season – is a robust explanation for the East African Humid Period.

4.3. Mechanisms contributing to a wetter dry season

What caused wetter conditions in East Africa from June–November? Our model simulations suggest that a change in the zonal advection of moisture from both the Atlantic and Indian Ocean basins was the most important contributing factor. On the Atlantic side, enhanced low pressure over North Africa during JJA at 6K in combination with the development of a dipole SST anomaly in the tropical Atlantic (Fig. 6A) leads to anomalously cyclonic conditions and weaker trade winds (also cf. Kutzbach and Liu, 1997; Zhao et al., 2007). As a result, there is an increase in westerly moisture flux into North and tropical Africa (i.e., an intensified West African monsoon) as well as enhanced convergence along the CAB (Fig. 6B). This westerly flux of moisture near to and south of the equator intensifies during SON (Fig. 6B), when anomalously low pressure over South Africa enhances the land–sea pressure gradient (Fig. 6A). The low develops in response to the heating of the southern half of the African continent, which receives ca. 5% greater incident solar radiation from June–November at 6K. By SON, the surface air temperature anomaly over South Africa reaches 1–1.5 °C. Meanwhile, cool SSTs (ca. 0.5–1 °C cooler than simulated 0K SSTs; Fig. 6A) that developed in response to reduced heating from December–May persist in the equatorial and southern tropical Atlantic Ocean. The temperature difference feeds a pressure differential (Fig. 6A), which further weakens the trade winds. This delivers more precipitation to the western branch of the East African Rift Valley, via enhanced convergence along the CAB (Fig. 6B).

The proxy isotopic reconstructions (Fig. 2B) afford the possibility to test this mechanism. Today, the isotopic composition of the Atlantic Ocean-derived precipitation in the Congo Basin is more depleted (ca. −25‰) than the composition of Indian Ocean-derived precipitation falling at Lake Challa (ca. −10‰). Lake Tanganyika, situated in between these two end-member sites, can receive precipitation from

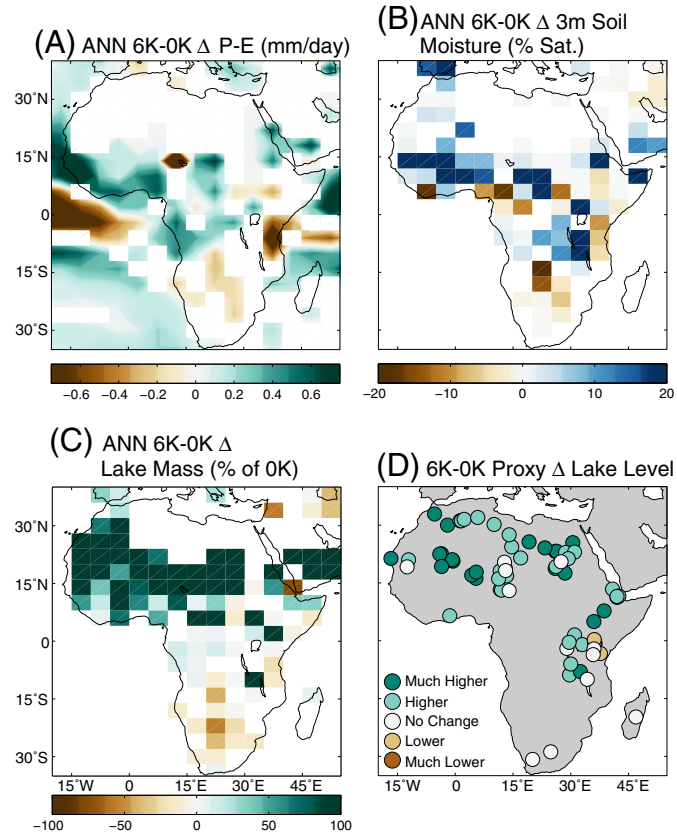

Fig. 5. (A) Simulated annual 6K–0K change in Precipitation–Evaporation in Africa. (B) Simulated 6K–0K change in annual soil moisture at 3 m in units of percent saturation. (C) Simulated 6K–0K change in lake mass, expressed as a percentage of 0K lake mass such that a 100% increase indicates a doubling of lake mass. (D) 6K–0K change in lake levels inferred from proxy data. For the simulated values, only differences significant at the 95% confidence level are shown.

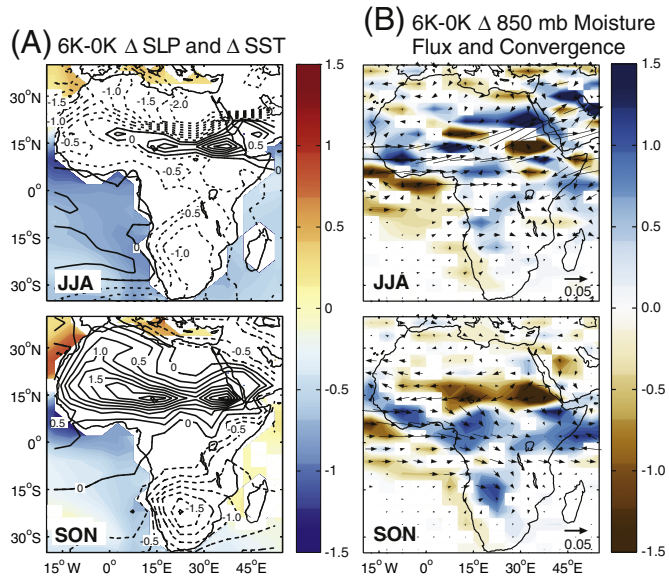

Fig. 6. (A) Simulated 6K–0K change in sea level pressure (SLP; line contours; mb) and sea surface temperature (SST; colored contours; degrees C) (B) Simulated 6K–0K change in 850 mb moisture flux (vectors; kg kg^{-1} m s^{-1}) and moisture flux convergence (colors; 10^{-3} kg kg^{-1} s^{-1}). Only differences significant at the 95% confidence level are shown.

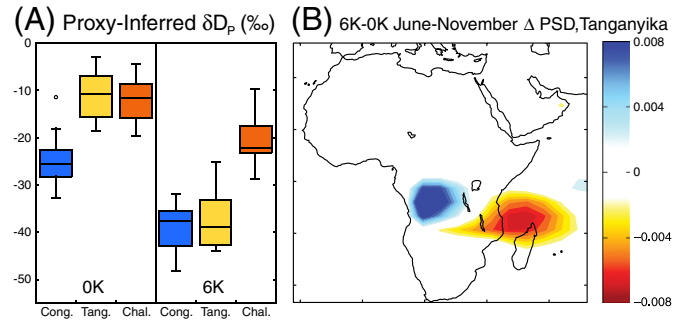

Fig. 7. (A) Proxy-inferred estimates of δD_P at 0K and 6K: data in Fig. 2B were binned from 3K–0K (0K) and 7 K–5 K (6K). Congo = Congo Basin, Tang. = Lake Tanganyika, Chal. = Lake Challa. All three sites show significant ($p<0.01$) depletion at 6K relative to the 0K bin (Student's t test). δD_P at Lake Tanganyika (in yellow) shows a shift from a composition similar to Challa at 0K to a composition similar to the Congo Basin at 6K. (B) Simulated 6K–0K precipitation source distribution (PSD) anomalies for the gridcell nearest to Lake Tanganyika (−6°S, 27.5°E) suggest a greater contribution of Congo moisture from June–November (in blue), in agreement with the proxy isotope data, and less moisture advection from the Indian Ocean (in red). The precipitation source distributions are unitless probability density functions normalized by the maximum probability density.

either the Congo Basin or easternmost Africa. The proxy reconstructions show that throughout the Late Holocene, δD_P at Lake Tanganyika was very similar to that of Lake Challa, suggesting that the majority of precipitation falling at Tanganyika originated from easternmost Africa (Fig. 7A). In contrast, at 6K Lake Tanganyika δD_P is far more depleted (−27‰ lighter than 0K values) and closely resembles the inferred 6K δD_P within the Congo Basin (Fig. 7A). This suggests that Congo Basin-derived moisture predominantly contributed to increased precipitation in the Lake Tanganyika Basin during the mid-Holocene, in agreement with the simulated moisture flux anomalies. Our PSD simulation results provide further support for this scenario, as they show a clear shift in the precipitation source distribution from June–November for the Tanganyika basin at 6K relative to 0K (Fig. 7B). Both model and proxy data indicate that the large depletion in the isotopic composition of precipitation near Lake Tanganyika at 6K is diagnostic of a change in precipitation source rather than exclusively a reflection of increased rainfall amount as was previously argued (Tierney et al., 2008). This interpretation is consistent with the suggestion of Lewis et al. (2010) that changes in the isotopes of precipitation at Lake Tanganyika during Heinrich Events also primarily reflect a shift in moisture source.

In addition to changes in hydrology caused by zonal advection of moisture from the Atlantic Ocean, there is an increase in convergence and rainfall in the Horn of Africa and easternmost Africa at 6K far east of the CAB (Fig. 6B), reflecting a contribution of excess moisture from the Indian Ocean to these particular areas. During JJA, surface wind speeds over the western Indian Ocean and the Bay of Bengal decrease at 6K relative to present-day velocities, while wind speeds farther north over the Arabian Peninsula slightly increase (Fig. 8A). These wind anomalies represent a northward shift of the southwesterly winds associated with the Indian Summer Monsoon. The decrease in wind speed over the western Indian Ocean reduces evaporation over this region and feeds the development of a warm SST anomaly, beginning in JJA (Fig. 8B) but maturing – due to the thermal inertia of the ocean – in SON (Fig. 8C). The warm SSTs in the west reduce the SST gradient across the Indian Ocean, weaken Walker circulation and cause a large increase in convergence and rainfall over the western Indian Ocean and into East Africa (Fig. 8D). This mechanism is the primary way by which areas within easternmost coastal Africa and the Horn of Africa – which are orographically isolated from the CAB – receive more rainfall at 6K.

The majority of coupled climate models participating in the Paleoclimate Model Intercomparison Project 2 (PMIP2) simulate a similar east–west dipole anomaly pattern in Indian Ocean SST and precipitation in the boreal fall at 6K (Zhao et al., 2005), indicating that the GISS ModelE-R results described here are robust, and reflect a fundamental impact of changing insolation on Indian Ocean monsoon circulation. As Zhao et al. (2005) have observed, this dipole structure at 6K is reminiscent of Indian Ocean Dipole (IOD) events in the present-day. In GISS ModelE-R, the precipitation anomaly pattern in particular is qualitatively similar to precipitation anomaly pattern typical of a positive IOD event (Fig. 8D and F), although the SST anomaly patterns are somewhat different (Fig. 8C and E); SSTs are only mildly cooler in the eastern Indian Ocean. Most importantly, the mechanism responsible for the mean seasonal change in Indian Ocean configuration in the mid-Holocene is completely different from the coupled ocean–atmosphere interactions responsible for individual IOD events, and thus the mean state in SON climatology does not necessarily reflect more frequent IOD events. Abram et al. (2007) postulated, based on fossil coral evidence from the eastern Indian Ocean, that IOD events in the mid-Holocene were stronger and more prolonged and that this was related to the mean state configuration of the Indian Ocean. On the other hand, Zhao et al. (2005) observed that in coupled models with the ability to simulate IOD-like variability, interannual IOD intensity was actually reduced at 6K as a consequence of the mean state change in boreal fall. GISS ModelE-R does not accurately simulate IOD events (Saji et al., 2006), so we cannot confidently assess within our results whether IOD event frequency or duration changed in response to the mean seasonal changes. However, from the perspective of hydrology in East Africa, the mean state change appears sufficient to increase seasonal P–E.

5. Conclusions

Our simulations of African hydrology at 6K indicate that the East African Humid Period was caused by a change in dry and "short rains" season precipitation and the subsequent reduction in precipitation seasonality. The simulated changes in lake mass and soil moisture are consistent with both the pollen and lake level paleodata from East Africa. The change in precipitation seasonality at 6K is a

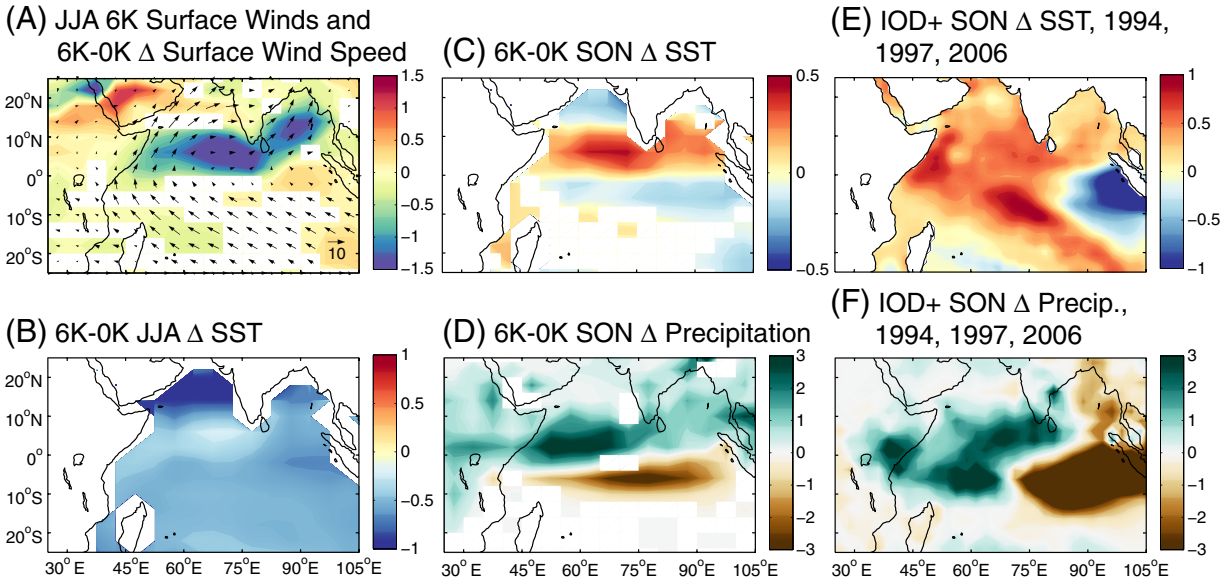

Fig. 8. (A) JJA surface winds at 6K (vectors; m/s) and 6K–0K wind speed anomalies (colors; m/s). A decrease in wind speed over the western Indian Ocean and the Bay of Bengal contributes to warmer SSTs, beginning in JJA (B) and maturing in SON (C). The warm SSTs increase precipitation rates in the western Indian Ocean and East Africa (D). Only differences significant at the 95% confidence level are shown. The 6K SON SST and precipitation anomalies are qualitatively similar to the anomaly patterns characteristic of Indian Ocean Dipole events (E and F; composite Reynolds-Smith SST (Reynolds et al., 2002) and Climate Prediction Center Merged Analysis of Precipitation (CMAP; Xie and Arkin, 1996) anomalies for three positive IOD years).

straightforward response of the climate system to changing seasonal insolation, and therefore the EAHP is indeed consistent with orbital expectations. However, unlike North Africa, where increased insolation during the rainy season caused an intensification of the West African monsoon, in East Africa dry season insolation had a greater impact on hydroclimate than rainy season insolation.

The two primary mechanisms that account for the increase in mid-Holocene East African precipitation from June–November are 1) an increase in moisture transport into central Africa from the Atlantic due to weakened trade winds and the development of low pressure over South Africa, and 2) an increase in precipitation in the Horn of Africa and easternmost Africa due to warmer SSTs in the western Indian Ocean. The anomalies associated with these processes are largest from September–November but are linked to dynamical changes occurring during boreal summer (June–August). In the Indian Ocean, the warm SST anomalies during the boreal fall are a seasonally-lagged response to the change in boreal summer surface winds associated with the Indian monsoon. In the Atlantic, the intensified West African monsoon and heating of the southern half of the African continent from June–August primes the system for the development of westerly moisture flux anomalies from September–November. These seasonally-lagged links between East African hydroclimate and boreal summer insolation may explain why Late Quaternary proxy records of hydrology in East Africa appear to be in-phase with Northern Hemisphere summer insolation, even in the southern tropics (Tierney et al., 2008).

The isotopic proxy data at Lake Tanganyika and the precipitation source tracers support our assertion based on the simulated dynamical changes that a deeper incursion of Atlantic moisture from September–November caused increased precipitation in the western Rift Valley during the mid-Holocene. Isotopic proxy data from the Congo Basin and Lake Challa show excellent agreement with model-simulated changes in δD_P from June–November, either suggesting a seasonal bias of the δD_{wax} proxy or that the model imperfectly captures changes in mean annual δD_P. Both improvement in the simulation of the isotopes of precipitation over tropical Africa and a better understanding of the seasonality of the δD_{wax} proxy in this region would be needed to ascertain which scenario is more likely.

This study also emphasizes that movement in ITCZ position had relatively little impact on Holocene East African hydrology for the timescale considered here. In agreement with previous modeling studies (Liu et al., 2004), our simulations suggest that reduced precipitation from December–May in both East and South Africa was caused by the cooling of the continent during the boreal winter and an increase in offshore transfer of precipitation, not by a shift in the ITCZ over land. Areas in Africa that are drier on a mean annual basis at 6K are those that do not receive excess rainfall from June–November, e.g. areas south of 10°S that have a more concentrated rainy season from December–February. This is broadly consistent with proxy reconstructions which have identified 10°S as the "hinge zone" in East Africa across which hydrological anomalies in the early to mid-Holocene change sign (Gasse, 2000). Thus, aridity south of the "hinge zone" is not caused by a mean northwards shifts in the position of the ITCZ, but is instead more likely due to the large reduction in December–March precipitation caused by continental cooling. Our study clearly shows that changes in zonal, not meridional, moisture flux were primarily responsible for changes in East African Holocene hydrology, highlighting the importance of considering mechanisms beyond ITCZ movement in the interpretation of past changes in terrestrial monsoonal climates.

Acknowledgements

We would like to thank NASA GISS for institutional support, and two anonymous reviewers whose comments greatly improved the manuscript. This research was supported by the NOAA/UCAR Climate and Global Change Postdoctoral Fellowship to JET and NSF ATM07-53868 to ANL. This is Lamont-Doherty Earth Observatory contribution number 7467.

References

Abram, N.J., Gagan, M.K., Liu, Z., Hantoro, W.S., McCulloch, M.T., Suwargadi, B.W., 2007. Seasonal characteristics of the Indian Ocean Dipole during the Holocene epoch. Nature 445, 299–302.

Adkins, J.F., deMenocal, P.B., Eshel, G., 2006. The "African humid period" and the record of marine upwelling from excess Th-230 in Ocean Drilling Program Hole 658C. Paleoceanography 21, PA4203.

Berger, A., Loutre, M., 1991. Insolation values for the climate of the last 10 million years. Quat. Sci. Rev. 10, 297–317.

Beuning, K.R.M., Russell, J.M., 2004. Vegetation and sedimentation in the Lake Edward Basin, Uganda–Congo during the late Pleistocene and early Holocene. J. Paleolimnol. 32, 1–18.

Brook, E., Harder, S., Severinghaus, J., Steig, E., Sucher, C., 2000. On the origin and timing of rapid changes in atmospheric methane during the last glacial period. Global Biogeochem. Cy. 14, 559–572.

Camberlin, P., Janicot, S., Poccard, I., 2001. Seasonality and atmospheric dynamics of the teleconnection between African rainfall and tropical sea-surface temperature: Atlantic vs. ENSO. Int. J. Climatol. 21, 973–1005.

Chikaraishi, Y., Naraoka, H., 2007. δ^{13}C and δD relationships among three *n*-alkyl compound classes (*n*-alkanoic acid, *n*-alkane and *n*-alkanol) of terrestrial higher plants. Org. Geochem. 38, 198–215.

Craig, H., Dixon, F., Craig, V., Edmond, J., Coulter, G., 1974. Lake Tanganyika geochemical and hydrographic study: 1973 expedition. Publication of Scripps Institution of Oceanography 75, pp. 1–83.

deMenocal, P.B., Ortiz, J., Guilderson, T., Adkins, J.F., Sarnthein, M., Baker, L., Yarusinsky, M., 2000. Abrupt onset and termination of the African Humid Period: rapid climate responses to gradual insolation forcing. Quat. Sci. Rev. 19, 347–361.

Feakins, S., Sessions, A., 2010. Controls on the D/H ratios of plant leaf waxes in an arid ecosystem. Geochim. Cosmochim. Acta 74, 2128–2141.

Finney, B., Johnson, T., 1991. Sedimentation in Lake Malawi (East Africa) during the past 10,000 years: a continuous paleoclimatic record from the southern tropics. Palaeogeogr. Palaeoclimatol. Palaeoecol. 85, 351–366.

Gasse, F., 2000. Hydrological changes in the African tropics since the Last Glacial Maximum. Quat. Sci. Rev. 19, 189–211.

Goddard, L., Graham, N.E., 1999. Importance of the Indian Ocean for simulating rainfall anomalies over eastern and southern Africa. J. Geophys. Res. 104, 19099–19116.

Gritti, E.S., Cassignat, C., Flores, O., Bonnefille, R., Chalié, F., Guiot, J., Jolly, D., 2010. Simulated effects of a seasonal precipitation change on the vegetation in tropical Africa. Clim. Past 6, 169–178.

Hansen, J., Sato, M., Ruedy, R., Kharecha, P., Lacis, A., Miller, R., Nazarenko, L., Lo, K., Schmidt, G., Russell, G., Aleinov, I., Bauer, S., Baum, E., Cairns, B., Canuto, V., Chandler, M., Cheng, Y., Cohen, A., Del Genio, A., Faluvegi, G., Fleming, E., Friend, A., Hall, T., Jackman, C., Jonas, J., Kelley, M., Kiang, N., Koch, D., Labow, G., Lerner, J., Menon, S., Novakov, T., Oinas, V., Perlwitz, J., Perlwitz, J., Rind, D., Romanou, A., Schmunk, R., Shindell, D., Stone, P., Sun, S., Streets, D., Tausnev, N., Thresher, D., Unger, N., Yao, M., Zhang, S., 2007. Climate simulations for 1880–2003 with GISS ModelE. Clim. Dyn. 29, 661–696.

Haug, G.H., Hughen, K.A., Sigman, D.M., Peterson, L.C., Rohl, U., 2001. Southward migration of the intertropical convergence zone through the Holocene. Science 293, 1304–1308.

Hou, J., D'Andrea, W.J., Huang, Y., 2008. Can sedimentary leaf waxes record D/H ratios of continental precipitation? Field, model, and experimental assessments. Geochim. Cosmochim. Acta 72, 3503–3517.

IAEA/WMO, 2006. Global Network of Isotopes in Precipitation. The GNIP Database. Accessible at: http://www.iaea.org/water.

Indermühle, A., Stocker, T.F., Joos, F., Fischer, H., Smith, H.J., Wahlen, M., Deck, B., Mastroianni, D., Tschumi, J., Blunier, T., Meyer, R., Stauffer, B., 1999. Holocene carbon-cycle dynamics based on CO_2 trapped in ice at Taylor Dome, Antarctica. Nature 398, 121–126.

Jolly, D., Taylor, D., Marchant, R., Hamilton, A., Bonnefille, R., Buchet, G., Riollet, G., 1997. Vegetation dynamics in central Africa since 18,000 yr BP: pollen records from the interlacustrine highlands of Burundi, Rwanda and western Uganda. J. Biogeogr. 24, 492–512.

Jolly, D., Prentice, I., Bonnefille, R., Ballouche, A., Bengo, M., Brenac, P., Buchet, G., Burney, D., Cazet, J., Cheddadi, R., et al., 1998. Biome reconstruction from pollen and plant macrofossil data for Africa and the Arabian peninsula at 0 and 6000 years. J. Biogeogr. 25, 1007–1027.

Kalnay, E., Kanamitsu, M., Kistler, R., Collins, W., Deaven, D., Gandin, L., Iredell, M., Saha, S., White, G., Woollen, J., Zhu, Y., Chelliah, M., Ebisuzaki, W., Higgins, W., Janowiak, J., Mo, K.C., Ropelewski, C., Wang, J., Leetma, A., Reynolds, R., Jenne, R., Joseph, D., 1996. The NCEP/NCAR 40-year reanalysis project. B. Am. Meteorol. Soc. 77, 437–471.

Kendall, R.L., 1969. An ecological history of the Lake Victoria basin. Ecol. Monogr. 39, 121–176.

Koster, R., Jouzel, J., Suozzo, R., Russell, G., Broecker, W., Rind, D., Eagleson, P., 1986. Global sources of local precipitation as determined by the NASA/GISS GCM. Geophys. Res. Lett. 13, 121–124.

Kröpelin, S., Verschuren, D., Lezine, A.M., Eggermont, H., Cocquyt, C., Francus, P., Cazet, J.P., Fagot, M., Rumes, B., Russell, J.M., Darius, F., Conley, D.J., Schuster, M., von Suchodoletz, H., Engstrom, D.R., 2008. Climate-driven ecosystem succession in the Sahara: the past 6000 years. Science 320, 765–768.

Kutzbach, J.E., Liu, Z., 1997. Response of the African monsoon to orbital forcing and ocean feedbacks in the middle Holocene. Science 278, 440–443.

Kutzbach, J.E., Otto-Bliesner, B.L., 1982. The sensitivity of the African–Asian monsoonal climate to orbital parameter changes for 9000 years BP in a low-resolution general circulation model. J. Atmos. Sci. 39, 1177–1188.

LeGrande, A.N., Schmidt, G.A., 2009. Sources of Holocene variability of oxygen isotopes in paleoclimate archives. Clim. Past 5, 441–455.

Levin, N., Zipser, E., Cerling, T., 2009. Isotopic composition of waters from Ethiopia and Kenya: insights into moisture sources for eastern Africa. J. Geophys. Res. 114, D23306.

Lewis, S.C., LeGrande, A.N., Kelley, M., Schmidt, G.A., 2010. Water vapour source impacts on oxygen isotope variability in tropical precipitation during Heinrich events. Clim. Past 6, 325–343.

Liu, Z., Harrison, S., Kutzbach, J., Otto-Bliesner, B., 2004. Global monsoons in the mid-Holocene and oceanic feedback. Clim. Dyn. 22, 157–182.

Liu, Z., Wang, Y., Gallimore, R., Gasse, F., Johnson, T.C., deMenocal, P.B., Adkins, J.F., Notaro, M., Prenticer, I.C., Kutzbach, J., Jacob, R., Behling, P., Wang, L., Ong, E., 2007. Simulating the transient evolution and abrupt change of Northern Africa atmosphere–ocean–terrestrial ecosystem in the Holocene. Quat. Sci. Rev. 26, 1818–1837.

Mapande, A.T., Reason, C.J.C., 2005. Interannual rainfall variability over western Tanzania. Int. J. Climatol. 25, 1355–1368.

McInerney, F.A., Helliker, B.R., Freeman, K.H., 2011. Hydrogen isotope ratios of leaf wax *n*-alkanes in grasses are insensitive to transpiration. Geochim. Cosmochim. Acta 75, 541–554.

Mitchell, T., Jones, P., 2005. An improved method of constructing a database of monthly climate observations and associated high-resolution grids. Int. J. Climatol. 25, 693–712.

Neinhuis, C., Barthlott, W., 1997. Characterization and distribution of water-repellent, self-cleaning plant surfaces. Ann. Bot. 79, 667–677.

Nicholson, S.E., 1996. A review of climate dynamics and climate variability in Eastern Africa. In: Johnson, T.C., Odada, E.O. (Eds.), The Limnology, Climatology and Paleoclimatology of the East African Lakes. Gordon and Breach, Amsterdam, pp. 25–56.

Nicholson, S.E., Kim, E., 1997. The relationship of the El Niño Southern Oscillation to African rainfall. Int. J. Climatol. 17, 117–135.

Peyron, O., Jolly, D., Bonnefille, R., Vincens, A., Guiot, J., 2000. Climate of east Africa 6000 C–14 yr BP as inferred from pollen data. Quat. Res. 54, 90–101.

Peyron, O., Jolly, D., Braconnot, P., Bonnefille, R., Guiot, J., Wirrmann, D., Chalié, F., 2006. Quantitative reconstructions of annual rainfall in Africa 6000 years ago: model-data comparison. J. Geophys. Res. 111, D24110.

Polissar, P., Freeman, K., 2010. Effects of aridity and vegetation on plant-wax δD in modern lake sediments. Geochim. Cosmochim. Acta 74, 5785–5797.

Renssen, H., Brovkin, V., Fichefet, T., Goosse, H., 2006. Simulation of the Holocene climate evolution in Northern Africa: the termination of the African Humid Period. Quat. Int. 150, 95–102.

Reynolds, R., Rayner, N., Smith, T., Stokes, D., Wang, W., 2002. An improved in situ and satellite SST analysis for climate. J. Clim. 15, 1609–1625.

Ritchie, J.C., Eyles, C.H., Haynes, C.V., 1985. Sediment and pollen evidence for an early to mid-Holocene humid period in the eastern Sahara. Nature 314, 352–355.

Rozanski, K., Araguás-Araguás, L., Gonfiantini, R., 1993. Isotopic patterns in modern global precipitation. In: Savin, S. (Ed.), Climate Change in Continental Isotopic Records. American Geophysical Union, Washington, DC, pp. 1–36.

Russell, J.M., Johnson, T.C., Kelts, K.R., Laerdal, T., Talbot, M.R., 2003. An 11,000-year lithostratigraphic and paleohydrologic record from Equatorial Africa: Lake Edward, Uganda–Congo. Palaeogeogr. Palaeoclimatol. Palaeoecol. 193, 25–49.

Sachse, D., Radke, J., Gleixner, G., 2004. Hydrogen isotope ratios of recent lacustrine sedimentary *n*-alkanes record modern climate variability. Geochim. Cosmochim. Acta 68, 4877–4889.

Sachse, D., Gleixner, G., Wilkes, H., Kahmen, A., 2010. Leaf wax *n*-alkane δD values of field-grown barley reflect leaf water δD values at the time of leaf formation. Geochim. Cosmochim. Acta 74, 6741–6750.

Saji, N.H., Goswami, B.N., Vinayachandran, P.N., Yamagata, T., 1999. A dipole mode in the tropical Indian Ocean. Nature 401, 360–363.

Saji, N.H., Xie, S.P., Yamagata, T., 2006. Tropical Indian Ocean variability in the IPCC twentieth-century climate simulations. J. Clim. 19, 4397–4417.

Schefuß, E., Schouten, S., Schneider, R.R., 2005. Climatic controls on central African hydrology during the past 20,000 years. Nature 437, 1003–1006.

Schmidt, G., Hoffmann, G., Shindell, D., Hu, Y., 2005. Modeling atmospheric stable water isotopes and the potential for constraining cloud processes and stratosphere–troposphere water exchange. J. Geophys. Res. 110, D21314.

Schmidt, G.A., Ruedy, R., Hansen, J.E., Aleinov, I., Bell, N., Bauer, M., Bauer, S., Cairns, B., Canuto, V., Cheng, Y., Del Genio, A., Faluvegi, G., Friend, A.D., Hall, T.M., Hu, Y., Kelley, M., Kiang, N.Y., Koch, D., Lacis, A.A., Lerner, J., Lo, K.K., Miller, R.L., Nazarenko, L., Oinas, V., Perlwitz, J., Perlwitz, J., Rind, D., Romanou, A., Russell, G.L., Sato, M., Shindell, D.T., Stone, P.H., Sun, S., Tausnev, N., Thresher, D., Yao, M.S., 2006. Present-day atmospheric simulations using GISS ModelE: comparison to in situ, satellite, and reanalysis data. J. Clim. 19, 153–192.

Schmidt, G., LeGrande, A., Hoffmann, G., 2007. Water isotope expressions of intrinsic and forced variability in a coupled ocean–atmosphere model. J. Geophys. Res. 112, D10103.

Shanahan, T.M., Overpeck, J.T., Wheeler, C.W., Beck, J.W., Pigati, J.S., Talbot, M.R., Scholz, C.A., Peck, J.A., King, J.W., 2006. Paleoclimatic variations in West Africa from a record of late Pleistocene and Holocene lake level stands of Lake Bosumtwi, Ghana. Palaeogeogr. Palaeoclimatol. Palaeoecol. 242, 287–302.

Sinninghe Damsté, J.S., Verschuren, D., Ossebaar, J., Blokker, J., van Houten, R., van der Meer, M.T.J., Plessen, B., Schouten, S., 2011. A 25,000-year record of climate-induced changes in lowland vegetation of eastern equatorial East Africa revealed by the stable carbon-isotopic composition of fossil plant leaf waxes. Earth Planet. Sci. Lett. 302, 236–246.

Smith, F.A., Freeman, K.H., 2006. Influence of physiology and climate on δD of leaf wax *n*-alkanes from C_3 and C_4 grasses. Geochim. Cosmochim. Acta 70, 1172–1187.

Sowers, T., Alley, R., Jubenville, J., 2003. Ice core records of atmospheric N_2O covering the last 106,000 years. Science 301, 945–948.

Stager, J.C., 1988. Environmental changes at Lake Cheshi, Zambia since 40,000 years BP. Quat. Res. 29, 54–65.

Stager, J., Cumming, B., Meeker, L., 2003. A 10,000-year high-resolution diatom record from Pilkington Bay, Lake Victoria, East Africa. Quat. Res. 59, 172–181.

Street, F.A., Grove, A.T., 1979. Global maps of lake-level fluctuations since 30,000 yr BP. Quat. Res. 12, 83–118.
Street-Perrott, F.A., Marchand, D.S., Roberts, N., Harrison, S.P., 1989. Global lake-level variations from 18,000 to 0 years ago: a paleoclimatic analysis. U.S. Department of Energy Technical Report 46, p. 20545. Washington, DC.
Talbot, M., Laerdal, T., 2000. The Late Pleistocene–Holocene palaeolimnology of Lake Victoria, East Africa, based upon elemental and isotopic analyses of sedimentary organic matter. J. Paleolimnol. 23, 141–164.
Tierney, J.E., Russell, J.M., Huang, Y., Sinninghe Damsté, J.S., Hopmans, E.C., Cohen, A.S., 2008. Northern hemisphere controls on tropical southeast African climate during the past 60,000 years. Science 322, 252–255.
Tierney, J.E., Russell, J.M., Huang, Y., 2010. A molecular perspective on Late Quaternary climate and vegetation change in the Lake Tanganyika basin, East Africa. Quat. Sci. Rev. 29, 787–800.
Tierney, J.E., Russell, J.M., Sinninghe Damsté, J.S., Huang, Y., Verschuren, D., 2011. Late Quaternary behavior of the East African monsoon and the importance of the Congo Air Boundary. Quat. Sci. Rev. 30, 798–807.
Ummenhofer, C.C., Gupta, A.S., England, M.H., Reason, C.J.C., 2009. Contributions of Indian Ocean sea surface temperatures to enhanced East African rainfall. J. Clim. 22, 993–1013.
Verschuren, D., Sinninghe Damsté, J.S., Moernaut, J., Kristen, I., Blaauw, M., Fagot, M., Haug, G.H., 2009. Half-precessional dynamics of monsoon rainfall near the East African equator. Nature 462, 637–641.
Vincens, A., Chalié, F., Bonnefille, R., Guiot, J., Tiercelin, J.J., 1993a. Nouvelle séquence pollinique du Lac Tanganyika: 30,000 ans d'historie botanique et climatique du Bassin Nord. Rev. Palaeobot. Palynol. 78, 381–394.
Vincens, A., Chalié, F., Bonnefille, R., Guiot, J., Tiercelin, J.J., 1993b. Pollen-derived rainfall and temperature estimates from Lake Tanganyika and their implication for Late Pleistocene water levels. Quat. Res. 40, 343–350.
Vincens, A., Buchet, G., Williamson, D., Taieb, M., 2005. A 23,000 yr pollen record from Lake Rukwa (8 degrees S, SW Tanzania): new data on vegetation dynamics and climate in Central Eastern Africa. Rev. Palaeobot. Palynol. 137, 147–162.
Xie, P.P., Arkin, P.A., 1996. Analyses of global monthly precipitation using gauge observations, satellite estimates, and numerical model predictions. J. Clim. 9, 840–858.
Zhao, Y., Braconnot, P., Marti, O., Harrison, S., Hewitt, C., Kitoh, A., Liu, Z., Mikolajewicz, U., Otto-Bliesner, B., Weber, S., 2005. A multi-model analysis of the role of the ocean on the African and Indian monsoon during the mid-Holocene. Clim. Dyn. 25, 777–800.
Zhao, Y., Braconnot, P., Harrison, S., Yiou, P., Marti, O., 2007. Simulated changes in the relationship between tropical ocean temperatures and the western African monsoon during the mid-Holocene. Clim. Dyn. 28, 533–551.